

Enhanced quantum entanglement in the non-Markovian dynamics of biomolecular excitons

Michael Thorwart,^{1,2} Jens Eckel,¹ John H. Reina,³ and Stephan Weiss¹

¹*Institut für Theoretische Physik, Heinrich-Heine-Universität Düsseldorf, 40225 Düsseldorf, Germany*

²*Freiburg Institute for Advanced Studies (FRIAS), Universität Freiburg, 79104 Freiburg, Germany*

³*Departamento de Física, Universidad del Valle, A.A. 25360, Cali, Colombia*

(Dated: March 22, 2019)

We show that quantum coherence of biomolecular excitons can be maintained over exceedingly long times due to the constructive role of their non-Markovian protein-solvent environment. Using a numerically exact real-time path integral approach, we provide evidence that a sluggish quantum bath helps to sustain quantum entanglement of two pairs of Förster coupled excitons, in contrast to a Markovian environment. We consider the full crossover from a fast to a slow non-Markovian bath and from weak to strong system-bath coupling and show that a slow bath can generate robust entanglement. This entanglement persists to surprisingly high temperatures, even higher than the excitonic gap. Such a fully quantum mechanical feature is not found for a Markovian bath.

PACS numbers: 03.65.Yz, 03.67.Bg, 82.39.Jn

Quantum coherent dynamics at the initial stages of photosynthesis in complex biomolecular structures seems to promote the efficiency of energy transfer from the light-harvesting antenna complexes to the chemical reaction centers [1, 2, 3, 4]. This hypothesis has recently been boosted by experiments revealing long-lived quantum coherent excitonic dynamics in the energy transfer among bacteriochlorophyll complexes over a surprisingly long time of around 600 fs measured at 77 K [1]. In addition, electronic coherences between excited states in purple photosynthetic bacteria have been monitored in a two-color photon echo experiment [2]. Both works lead to the conclusion that the collective long-range electrostatic response of the biomolecular protein environment to the electronic excitations should be responsible for the long-lived quantum coherence. Furthermore, the obtained time scales [2] for the short-time dynamics of the nuclear modes coupled to the excitonic states of two chromophores are almost identical. This points to the special and constructive role of the quantum environment for the photoexcitations. The often assumed coupling of the chromophores to fast and independent quantum baths does not hold in this case. In fact, the two chromophores are embedded in the *same* protein-solvent environment. These results corroborate experimental studies [3] which show that energy transport sensitively depends on the spatial properties of the delocalized excited-state wave functions of the *whole* pigment-protein complex. In addition, there are reports of coherently controlled wave packet quantum dynamics artificially generated by laser pulses in the light-harvesting antenna of the bacteria *Rhodospseudomonas acidophila* [4].

An appropriate theoretical description of the biomolecular quantum dynamics has to account for the environmental time scales typically being of the same order of magnitude as the excitonic time scales [5]. This fact renders the dynamics highly non-Markovian and rather elaborate techniques are required to address the entire cross-over from fast to slowly responding baths.

Here, we perform a deterministic evaluation of real-time path integrals [6, 7] where all non-Markovian effects are exactly included. In so doing, we provide numerically exact results for the quantum coherent dynamics of photoexcitations in coupled chromophores, where the time evolution of the protein-solvent bath happens on time scales comparable to the exciton dynamics. We show that the non-Markovian effects help to sustain quantum coherence over rather long times. Furthermore, quantum entanglement [8] of two chromophore pairs is shown to be more stable under the influence of a non-Markovian bath. Even at high temperatures, a slow bath can generate a considerable degree of entanglement, a feature absent in the Markovian case. In passing, we mention that recently, quantum entanglement of two optical two-level systems coupled to a common localized environmental mode has been studied beyond the Markov approximation at zero temperature [9].

A single chromophore with index i can be modeled as a quantum two level system described by Pauli matrices $\tau_{x,y,z}^i$ with energy gap E_i between ground-state $|g_i\rangle$ and excited state $|e_i\rangle$ [5]. The protein-solvent environment is formalized as a bath of harmonic oscillators with a bilinear system-bath coupling yielding the standard spin-boson Hamiltonian for each chromophore [5]. The coupling between two chromophores is introduced as the dipole-like Förster term $H_{12} = \frac{\hbar\Delta}{2}(\tau_x^1\tau_x^2 + \tau_y^1\tau_y^2)$ [10]. Since the system's total number of excitations is a constant of motion, the two-chromophore system can be effectively reduced to a single spin-boson model of one chromophore pair described by the Pauli matrices $\sigma_{x,z}$:

$$H_1 = \frac{\hbar\epsilon}{2}\sigma_z + \frac{\hbar\Delta}{2}\sigma_x + \hbar\sigma_z \sum_{\kappa} c_{\kappa}(b_{\kappa}^{\dagger} + b_{\kappa}) + \sum_{\kappa} \hbar\omega_{\kappa} b_{\kappa}^{\dagger} b_{\kappa}, \quad (1)$$

where $\epsilon = E_1 - E_2$, and b_{κ} describe bosonic bath operators with couplings c_{κ} . We consider equal chromophores $E_1 = E_2$; the effective basis for a chromophore pair is given by $\{|\uparrow\rangle = |e_1g_2\rangle, |\downarrow\rangle = |g_1e_2\rangle\}$.

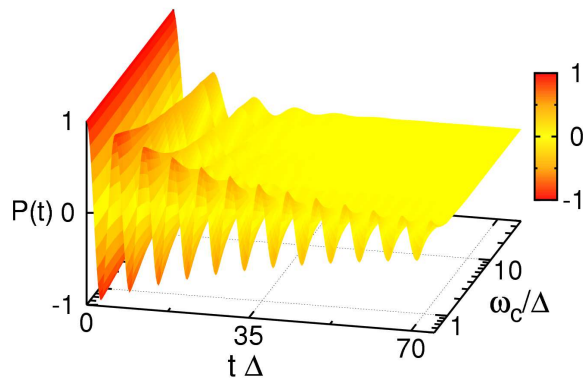


FIG. 1: Population difference $P(t)$ for a single chromophore pair and full cross-over from a Markovian to a non-Markovian responding bath. The time scale and the bath cut-off frequencies ω_c are in units of the pair Förster coupling Δ . The dynamics is calculated for $k_B T = 0.1\hbar\Delta$, and $\alpha = 0.1$.

The spectral density of the environment [11] follows from a microscopic derivation [12]. Different forms of a Debye dielectric can be assumed, but in any case, lead to an Ohmic spectral density $G(\omega) = 2\pi\alpha\omega e^{-\omega/\omega_c}$. The dimensionless damping constant α of the protein-solvent can be related to the parameters of the dielectric model [12]. One finds for the order of magnitude of $\alpha \sim 0.01 - 0.1$ [5, 12]. We use an exponential form of the cut-off at frequency ω_c . This sets the time-scale on which the dynamics of the bath evolves and is related to the reorganization energy $E_r \sim 2\alpha\hbar\omega_c$. If $\Delta \ll \omega_c$, the bath evolves fast compared to the system and loses its memory quickly, rendering a Markovian approximation and the standard Bloch-Redfield description [13] suitable. However, for the considered biomolecular environment, $\hbar\omega_c$ is typically of the order of $\sim 2 - 8$ meV, while the Förster coupling constants can range from $\hbar\Delta \sim 0.2$ meV–100 meV [5, 12]. Hence, the bath responds slower than the dynamics of the excitons evolve, and non-Markovian effects become dominant. Coherent oscillations in a strongly damped two-state system with $\alpha > 1$ and $\Delta \gtrsim \omega_c$ have been found using numerically exact quantum Monte Carlo simulations [14, 15] and by applying the numerical renormalization group [16].

Here, we use the quasiadiabatic propagator path-integral (QUAPI) [6, 7] to calculate the time-dependent reduced density matrix of the system. This allows the evaluation of the single chromophore pair dynamics by studying the population difference $P(t) = \langle \sigma_z \rangle_t$ [11]. As the initial condition, we choose $P(0) = 1$. Figure 1 shows the results for $\alpha = 0.1$. $P(t)$ decays with time in an oscillatory way. The decay occurs faster for large ω_c while for small ω_c , the sluggish bath sustains more coherent oscillations which persist even on the ps time scale in dimensionful units. In general, for smaller ω_c the spectral weight of the bath modes around the system frequency Δ is suppressed and the decohering influence is reduced, yielding prolonged coherence.

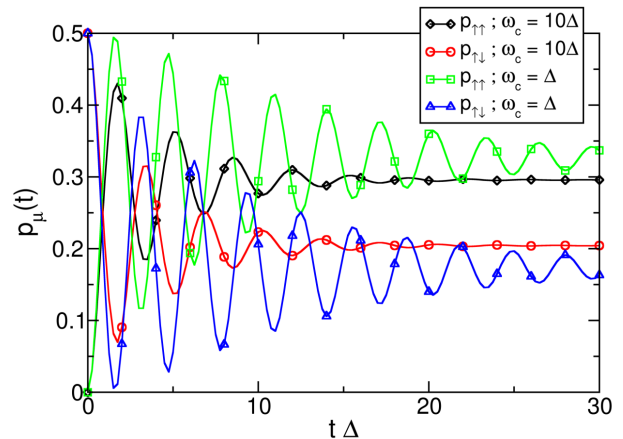


FIG. 2: Time evolution of the populations $p_\mu(t)$ for two coupled chromophore pairs. This illustrates the action of a slow ($\omega_c = \Delta$) and a fast ($\omega_c = 10\Delta$) bath, for $k_B T = 0.1\hbar\Delta$, $\alpha = 0.1$, and for interpair Förster coupling $J = 0.1\Delta$.

Next, we address entanglement between two chromophore pairs under the influence of a slow bath. We consider two equal pairs described by $\sigma_{x/z,i}$, coupled by an interpair Förster interaction J and coupled to a harmonic bath. The total Hamiltonian reads

$$H_2 = \sum_{i=1,2} \frac{\hbar\Delta}{2} \sigma_{x,i} + \hbar J (\sigma_{x,1} \sigma_{x,2} + \sigma_{y,1} \sigma_{y,2}) \quad (2)$$

$$+ \frac{\hbar}{2} (\sigma_{z,1} + \sigma_{z,2}) \sum_{\kappa} \tilde{c}_{\kappa} (b_{\kappa}^{\dagger} + b_{\kappa}) + \sum_{\kappa} \hbar\omega_{\kappa} b_{\kappa}^{\dagger} b_{\kappa},$$

whose basis refers to the states $\{|\uparrow_1\rangle = |e_1g_2\rangle, |\downarrow_1\rangle = |g_1e_2\rangle, |\uparrow_2\rangle = |e_3g_4\rangle, |\downarrow_2\rangle = |g_3e_4\rangle\}$. As before, the bath spectral density follows from a Debye dielectric model, again yielding the Ohmic form. The time-dependent reduced density matrix $\rho(t)$ is computed using an adapted QUAPI scheme. Figure 2 shows the time-evolution of the populations $p_{\uparrow\uparrow}(t) = p_{\downarrow\downarrow}(t)$ and $p_{\uparrow\downarrow}(t) = p_{\downarrow\uparrow}(t)$ of the four basis states for different values of ω_c for the initial preparation $|\psi_0\rangle = (|\uparrow_1\downarrow_2\rangle + |\downarrow_1\uparrow_2\rangle)/\sqrt{2}$. After a transient oscillatory behavior, the stationary equilibrium values are reached. The corresponding decay occurs on shorter times for large ω_c , i.e., fast baths, compared to the rather slow decay for small ω_c .

To quantify the two-pair quantum correlations, we study the entanglement along the negativity $N(t) = \max\{0, -2\zeta_{\min}(t)\}$ [17, 18], where $\zeta_{\min}(t)$ denotes the smallest eigenvalue of the partially transposed reduced density operator with the matrix elements $\rho_{m\mu, n\nu}^{T_2} = \rho_{n\mu, m\nu}$. A separable state has $N = 0$, while for a maximally entangled state, $N = 1$.

Figure 3(a) shows the time evolution of $N(t)$ for two different values $\omega_c = \Delta$, and $\omega_c = 50\Delta$, for the maximally entangled initial state $|\psi_0\rangle$. Starting from $N(0) = 1$ we observe a decay to zero with small oscillations superimposed. For the Markovian bath $\omega_c = 50\Delta$, the decay

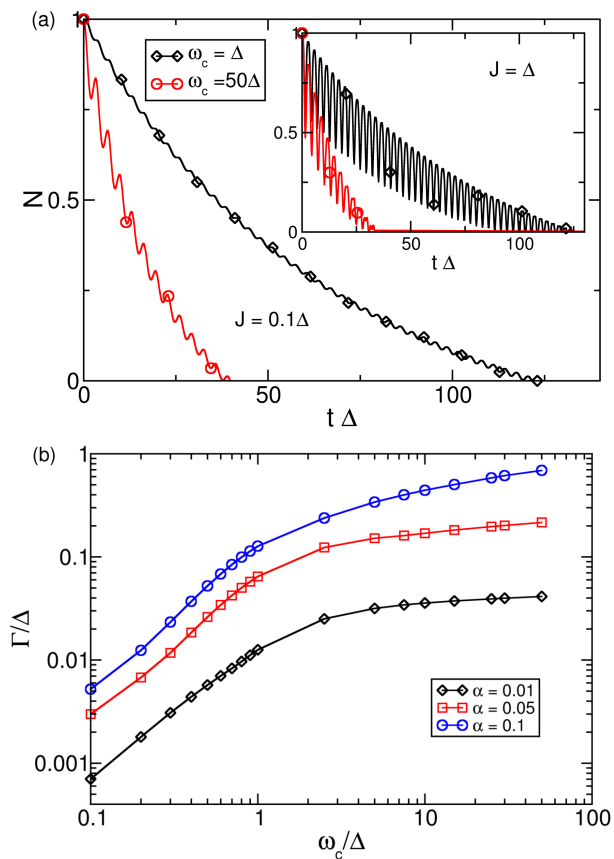


FIG. 3: (a) Time evolution of the negativity $N(t)$ for the cut-off frequencies $\omega_c = \Delta$ (black) and $\omega_c = 50\Delta$ (red) for the interpair Förster coupling $J = 0.1\Delta$ (main) and $J = \Delta$ (inset). Moreover, $k_B T = 0.1\hbar\Delta$. (b) Decay constant Γ as a function of the cut-off frequency ω_c for different values of α for $k_B T = 0.1\hbar\Delta$, $J = 0.1\Delta$.

occurs faster than for the non-Markovian bath $\omega_c = \Delta$ indicating that entanglement survives on a longer time scale for the slow bath as compared to the fast bath. For a larger interpair coupling $J = \Delta$, the superimposed oscillations are more pronounced (Fig. 3(a) inset) which is due to constructive interference of the involved transitions within the chromophore system. For a quantitative picture, we fit an exponential $N(t) = N_0 \exp(-\Gamma t) + N_1$ with a decay constant Γ which contains the influence of the bath. Figure 3(b) shows the dependence of Γ on ω_c . Clearly, Γ strongly decreases for small ω_c , while for large ω_c , the rate constant saturates. The dependence of Γ on ω_c is more pronounced for larger values of α . This nicely illustrates that entanglement is much more robust in biomolecular systems compared to other macroscopic condensed-matter devices [19] which display quantum coherent behavior.

To study the cross-over between fast and slow baths, we show $N(t)$ for varying ω_c in Fig. 4 for the initial state $|\psi_1\rangle = |\uparrow_1\uparrow_2\rangle$. Figure 4(a) shows the result for $J = 0.1\Delta$. The entanglement is rather quickly destroyed

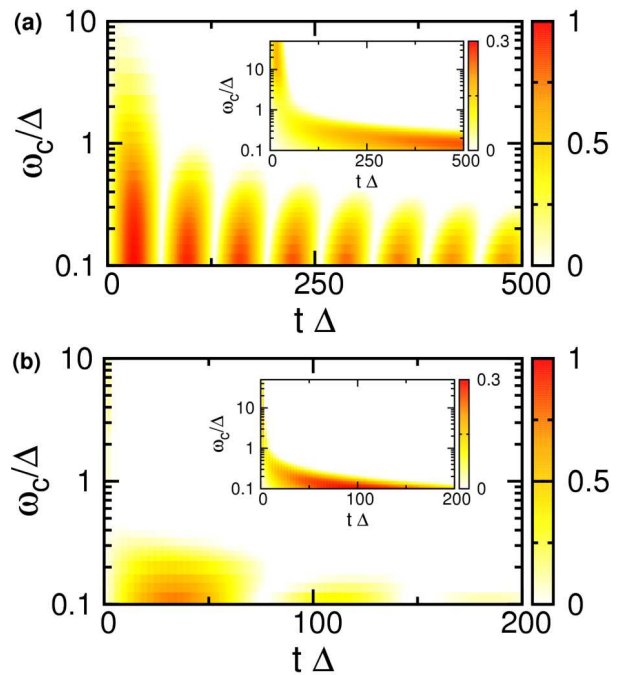


FIG. 4: (a) Negativity $N(t)$ as a function of ω_c for $J = 0.1\Delta$ (main) and $J = 0$ (inset), for $\alpha = 0.01$ and $k_B T = 0.1\hbar\Delta$. (b) Same as in (a), but for the strong coupling case $\alpha = 0.1$.

in the regime $\omega_c \gg \Delta$. On the other hand, we find a regular oscillatory decay for $0.1\Delta \lesssim \omega_c \lesssim \Delta$. In this regime, complete entanglement disappearance and revivals alternate. The time scale of the entanglement oscillations is given by $2\pi/J$. The constructive role of a sluggish bath is further illustrated in the inset of Fig. 4(a), where $N(t)$ is shown for $J = 0$. In fact, in the regime $\omega_c < \Delta$, we find that entanglement between the two pairs is generated by their common interaction with a sluggish bath. Most interestingly, for $\omega_c = 0.1\Delta$, $N(t)$ steadily grows even over rather long times up to $t\Delta = 500$. In view of the single-pair results described above, this seems counterintuitive since for small ω_c , a reduced influence of the bath modes would be expected. However, in this regime, the bath is rather efficient in generating entanglement. This feature survives even for larger values of α , see Fig. 4(b). The oscillatory behavior of the entanglement generation still occurs for $J = 0.1\Delta$, where $N(t)$ assumes all values between zero and one. The bath-induced destruction happens here earlier due to the large α . Entanglement is also produced when $J = 0$, see inset of Fig. 4(b), for $0.1\Delta \lesssim \omega_c \lesssim \Delta$. Also here, $N(t)$ can even reach the maximal value at intermediate times.

So far, we have studied not so high temperatures, similar to the experimental conditions in Refs. [1, 2]. However, in Fig. 5(a) (main) we plot $N(t)$ for varying ω_c , for $k_B T = \hbar\Delta$, for the initial state $|\psi_1\rangle$. We still find large entanglement oscillations at short to intermediate times, for $0.1\Delta \lesssim \omega_c \lesssim \Delta$ despite the rather large temperature: this is an outstanding hardware feature that could

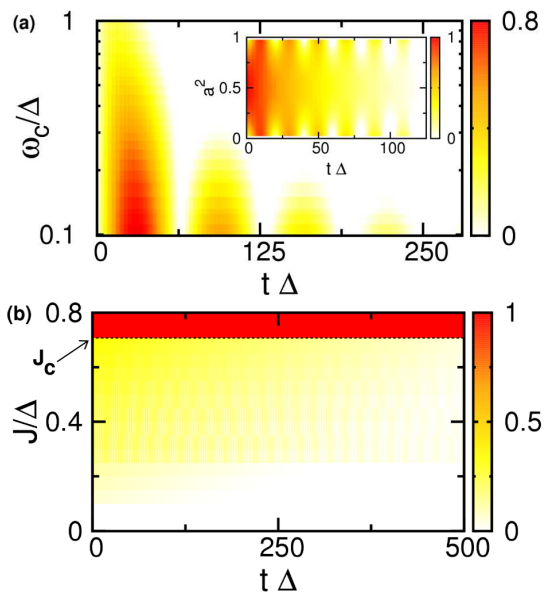


FIG. 5: Excitonic entanglement robustness: (a) Negativity $N(t)$ for varying ω_c ; $J = 0.1\Delta$, $\alpha = 0.01$ and $k_B T = \hbar\Delta$ (Main). Inset: $N(t)$ for different weights in the initial preparation $|\psi_2\rangle = a|\uparrow_1\downarrow_2\rangle + b|\downarrow_1\uparrow_2\rangle$, for $J = 0.1\Delta$, $\alpha = 0.01$, $k_B T = 0.1\hbar\Delta$, and $\omega_c = \Delta$. (b) $N(t)$ for varying J ; $\alpha = 0.01$, $k_B T = 0.1\hbar\Delta$, $\omega_c = 0.1\Delta$. The horizontal line marks the critical value $J_c = 1/\sqrt{2}$ above which the initially prepared ground state belongs to a DFS.

provide a useful resource for the artificial design of controlled, robust, and efficient biomolecular nanostructures for quantum information processing [8, 20, 21, 22].

Furthermore, we have varied the initial preparation to the state $|\psi_2\rangle = a|\uparrow_1\downarrow_2\rangle + b|\downarrow_1\uparrow_2\rangle$ with $a^2 + b^2 = 1$. The inset of Fig. 5(a) shows $N(t)$ for varying a^2 and

$J = 0.1\Delta$. $|\psi_2\rangle$ is maximally entangled for $a^2 = 1/2$, for which $N(t)$ decays monotonously with time, while away from this region the negativity again shows collapses and revivals. For the borders $a^2 \rightarrow 0, 1$, $|\psi_2\rangle$ is a separable state, but entanglement is rather quickly generated with time before it finally dies out. Robust entanglement thus depends on the initial preparation and is favored by the choice of initially separable (or weakly entangled) states.

Finally, we analyze the dependence on the interpair coupling J . The negativity $N(t)$ is shown in Fig. 5(b) for varying J for the respective ground state as the initial preparation. From Eq. (2) it follows that a critical value $J_c = 1/\sqrt{2}$ exists such that for $J \geq J_c$, the state $|\psi_g\rangle = (|\uparrow_1\downarrow_2\rangle - |\downarrow_1\uparrow_2\rangle)/\sqrt{2}$ is the two-pair groundstate, which, however, belongs to a decoherence-free subspace (DFS) of H_2 [23]. Hence, $N(t)$ remains constantly maximal. For $J < J_c$, the ground state has some weight outside of the DFS and hence suffers from decoherence.

The general nature of our results demonstrate that pure quantum mechanical effects provide the conditions for efficient light harvesting and therefore that the evolutionary process has led to a robust, ultrafast yet efficient quantum rule for photosynthetic processing. The results reported here are of direct relevance to quantum dot and molecular architectures [24, 25]. They could prove crucial in the design of artificial efficient light harvesters for robust multipartite biomolecular entanglement, with enhanced energy transfer rates [26] for the control and conditional dynamics [8, 22] of quantum bits.

We acknowledge support by the DFG priority program 1243, COLCIENCIAS grant 1106-14-17903, and by the DAAD-PROCOL Program. Computational time from the ZIM at the Heinrich-Heine-Universität Düsseldorf is also acknowledged.

-
- [1] G. S. Engel *et al.*, Nature **446**, 782 (2007).
[2] H. Lee, Y.-C. Cheng, and G. R. Fleming, Science **316**, 1462 (2007).
[3] T. Brixner *et al.*, Nature **434**, 625 (2005).
[4] J. L. Herek *et al.*, Nature **417**, 533 (2002).
[5] J. Gilmore and R. McKenzie, Chem. Phys. Lett. **421**, 266 (2006).
[6] N. Makri, J. Math. Phys. **36**, 2430 (1995); N. Makri *et al.* Proc. Natl. Acad. Sci. USA **93**, 3926 (1996).
[7] M. Thorwart *et al.*, Chem. Phys. **235**, 61 (1998).
[8] C. H. Bennett and D. P. DiVincenzo, Nature **404**, 247 (2000).
[9] B. Bellomo, R. Lo Franco, and G. Compagno, Phys. Rev. Lett. **99**, 160502 (2007).
[10] J. H. Reina, L. Quiroga, and N. F. Johnson, Phys. Rev. A **62**, 012305 (2000).
[11] U. Weiss, *Quantum Dissipative Systems*, 3rd ed. (World Scientific, Singapore, 2008).
[12] J. Gilmore and R. McKenzie, J. Phys. Chem. A **112**, 2162 (2008).
[13] V. May and O. Kühn, *Charge and energy transfer dynamics in molecular systems* (Wiley, Berlin, 2001).
[14] R. Egger, and C. H. Mak, Phys. Rev. B **50**, 15210 (1994).
[15] L. Mühlbacher and R. Egger, J. Chem. Phys. **118**, 179 (2003).
[16] R. Bulla *et al.*, Phys. Rev. B **71**, 045122 (2005).
[17] A. Peres, Phys. Rev. Lett. **77**, 1413 (1996).
[18] M. Horodecki, P. Horodecki, and R. Horodecki, Phys. Lett. A **223**, 1 (1996).
[19] Y. Makhlin, G. Schön, and A. Shnirman, Rev. Mod. Phys. **73**, 357 (2001).
[20] M. Kroutvar *et al.*, Nature **432**, 81 (2004).
[21] P. Rabl *et al.*, Phys. Rev. Lett. **97**, 033003 (2006).
[22] M. Thorwart and P. Hänggi, Phys. Rev. A **65**, 012309 (2002).
[23] J. H. Reina, L. Quiroga, and N. F. Johnson, Phys. Rev. A **65**, 032326 (2002).
[24] S. A. Crooker *et al.*, Phys. Rev. Lett. **89**, 186802 (2002).
[25] J. H. Reina *et al.*, Phys. Rev. Lett. **93**, 250501 (2004).
[26] K. Becker *et al.*, Nature Mater. **5**, 777 (2006).